JOURNAL OF MATERIALS SCIENCE 29 (1994) 3342–3350

Modelling of continuous recrystallization in aluminium alloys

M. T. LYTTLE, J. A. WERT
Department of Materials Science and Engineering, University of Virginia, Charlottesville, VA 22903, USA

Microstructure and microtexture analyses have been made of three aluminium alloys after annealing alone and after concurrent straining and annealing, and simulative models of microstructure/microtexture evolution processes have been formulated. Both experimental and modelling results are presented as boundary misorientation distributions. For each alloy, the results show that annealing alone does not significantly alter the boundary misorientation distribution, while concurrent straining and annealing (up to a strain of 0.5) decreases the fraction of low-angle boundaries. To understand the mechanisms by which concurrent straining and annealing alter the boundary misorientation distribution, three simulative models of microstructure/microtexture evolution during concurrent straining and annealing have been formulated. Application of the models to experimentally determined initial microstructure/microtexture states shows that the boundary sliding (sub)grain rotation model decreases the fraction of low-angle boundaries, the dislocation glide (sub)grain rotation model increases the fraction of low-angle boundaries, and the (sub)grain neighbour switching model has a modest effect on the boundary misorientation distribution. A combination of the boundary sliding (sub)grain rotation model and the (sub)grain neighbour switching model most closely reproduces the boundary misorientation distributions found experimentally.

1. Introduction

Continuous recrystallization refers to the process by which a deformation microstructure is converted into a grain structure, without the necessity for migration of high-angle boundaries. This process differs from discontinuous recrystallization in that nucleation and growth of new grains do not occur. Instead, low-angle boundaries in the recovering deformation microstructure evolve into high-angle boundaries as a result of subgrain rotation processes. The term "subgrain rotation" as conventionally used in the context of subgrain coalescence implies that lattice orientations in adjacent subgrains converge [1–4]. In the context of continuous recrystallization, subgrain rotation implies that lattice orientations in adjacent subgrains diverge.

When a deformation microstructure evolves into a recrystallized grain structure by gradual lattice rotations, an individual crystal may be bounded at various times by low-angle boundaries predominately, by a mixture of low- and high-angle boundaries, and finally by high-angle boundaries predominately. Rather than seeking to adapt the discreet terms "subgrain" and "grain" to this continuum of microstructural states, we use the term "(sub)grain" to refer to the individual crystals in all but the final recrystallized microstructure, where we refer to grains.

Texture measurements and boundary misorientation studies show that little spontaneous divergent (sub)grain rotation occurs during annealing of deformation microstructures [4, 5], implying that continuous recrystallization cannot take place during annealing alone. However, when a cold- or warm-rolled material is deformed at a slow strain rate at the annealing temperature, the applied stress apparently creates a driving force for (sub)grain rotation, and low-angle boundaries in the recovering deformation microstructure continuously evolve into high-angle boundaries. Thus, continuous recrystallization appears to be strictly a dynamic process, and the preponderance of detailed experimental observations relative to continuous recrystallization are associated with studies of superplastic deformation of aluminium alloys [6–26]. The conclusion that continuous recrystallization can only occur dynamically is consistent with the observation that low-angle boundary energy increases as boundary misorientation increases [27, 28]. Therefore, any process that leads to general divergence of (sub)grain orientations requires an external driving force, which is supplied by the applied stress during concurrent straining and annealing but which is absent during static annealing.

Despite the accumulation of evidence that a grain structure can evolve from a deformation microstructure through (sub)grain rotation driven by stress at elevated temperatures, the mechanism(s) that lead to (sub)grain rotation during concurrent straining and annealing have not been definitively identified. (Sub)grain boundary sliding, (sub)grain neighbour switching, and intra(sub)granular slip have all been suggested as mechanisms that contribute to continu-

0022–2461

ous recrystallization [13–26]. (Sub)grain growth has also been proposed as a continuous recrystallization mechanism [8–12], but (sub)grain growth without concurrent (sub)grain rotation is inconsistent with a variety of texture observations [21–26].

Essentially, all reports of continuous recrystallization describe microstructure, boundary misorientation, and/or texture at discrete strain intervals. *In situ* observations of the process of continuous recrystallization have not been reported. Absent direct observations of (sub)grain rotation processes, models that simulate (sub)grain rotation during concurrent straining and annealing could provide insight into the mechanisms of (sub)grain rotation that contribute to continuous recrystallization. The purpose of the present work was to describe simulative models of several possible mechanisms of (sub)grain rotation during concurrent straining and annealing, and to compare the model predictions with experimental observations of continuous recrystallization in three aluminium alloys.

2. Experimental observations

Grain orientation and boundary misorientation data for Al–0.24Zr–0.1Si and Al–4.1Cu–0.28Zr–0.1Si alloys (compositions are given in weight per cent) have been previously reported [21, 22] and are included in the present paper for comparison with model results. Similar experimental observations have been made more recently for a Weldalite^{tm} alloy designated 049 (Al–4.76Cu–1.27Li–0.37Ag–0.33Mg–0.13Zr) and are reported for the first time in the present paper. The techniques used for concurrent straining and annealing experiments have been described previously [21, 22], including specific temperatures, holding times, and initial strain rates for the Al–Zr–Si and Al–Cu–Zr–Si alloys. For the Al–Cu–Li–Ag–Mg–Zr alloy, tensile specimens with the tensile axis parallel to the rolling direction (L) were heated to the test temperature of 773 K in approximately 0.5 h, and were held at that temperature for 0.16 h prior to straining at an initial strain rate of $6.6 \times 10^{-4} s^{-1}$. Tests were interrupted at true strains, ε, of 0.11, 0.21 and 0.47; and the tensile specimens were rapidly quenched in water. TEM foils normal to the long transverse (T) direction were prepared, and measurements of grain orientation and boundary misorientation were performed as described previously [21, 22].

Experimental results consist of lattice orientation data for individual, contiguous (sub)grains; from which the axis/angle pairs for individual boundaries are extracted. Figs 1–3 show the distributions of the boundary misorientation angles from various samples, represented in the form of histograms.

The as-rolled microstructure has been evaluated for the Al–Zr–Si alloy. Approximately two-thirds of the boundaries characterized have misorientations of 10° or less. The boundaries with misorientations near 55° are transition-band-type boundaries between deformation bands, and are nearly always parallel to the rolling plane. Similar features have been described by other authors for a variety of rolled aluminium alloys [29–37].

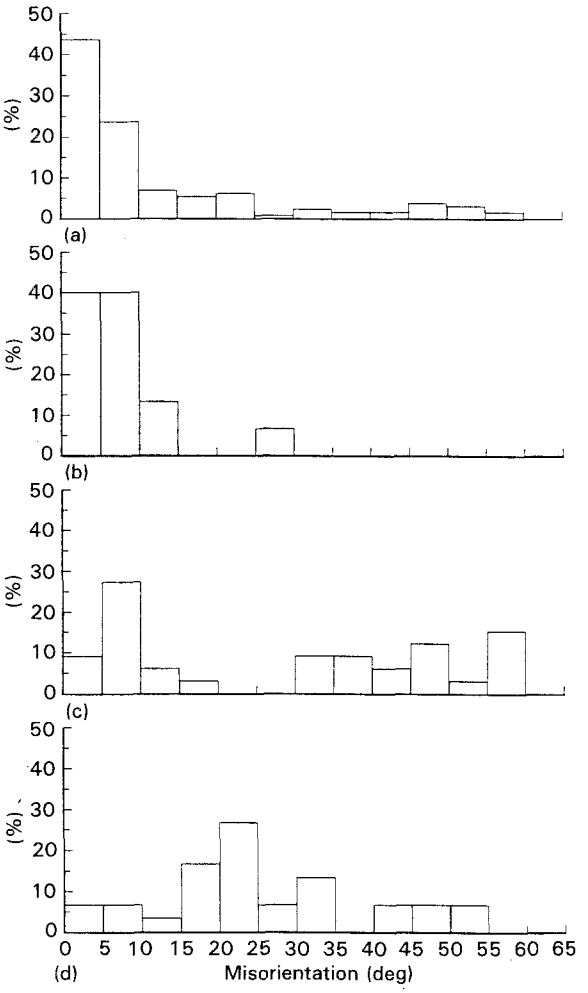

Figure 1 Experimentally determined boundary misorientation distributions for the grip and gauge sections of the Al–Zr–Si alloy. (a) As-rolled; (b) grip, strain = 0.22; (c) gauge, strain = 0.22; (d) gauge, strain = 0.46.

The grip section results are broadly similar for all three alloys investigated. More than half of the boundaries examined in each grip section have misorientations of 10° or less, similar to the as-rolled microstructure of the Al–Zr–Si alloy. Transition-band-type boundaries were observed in the Al–Cu–Zr–Si and Al–Cu–Li–Ag–Mg–Zr grip sections, but not in the Al–Zr–Si grip section. It is thought that this reflects the small number of observations and variable spacing of transition-band-type boundaries, rather than a fundamental difference between these microstructures. It has been previously reported that the boundary misorientation distributions in samples of the Al–Zr–Si alloy annealed for extended periods (not grip sections of tensile specimens) were essentially the same as the boundary misorientation distributions in the grip sections [21]. Taken as a whole, these results suggest that in the absence of discontinuous recrystallization, annealing without concurrent deformation does not significantly alter the boundary misorientation distribution in any of the three alloys investigated.

Figs 1–3 also show boundary misorientation distributions for the gauge sections of the tensile samples. These results are characterized by a marked decrease in the fraction of boundaries with misorientations of 10° or less, and a simultaneous increase in the fraction

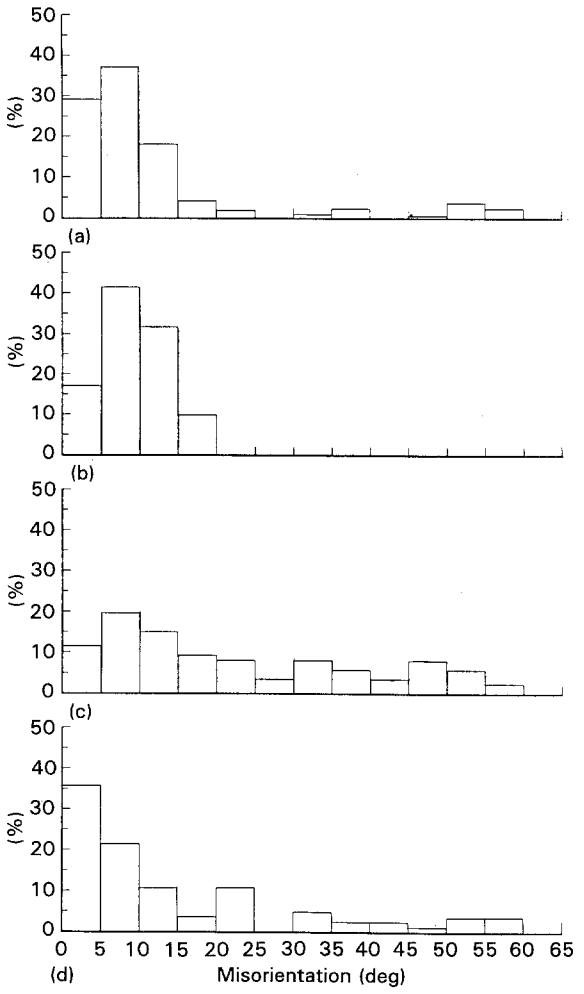

Figure 2 Experimentally determined boundary misorientation distributions for the grip and gauge sections of the Al–Cu–Zr–Si alloy. (a) Grip, strain = 0.22; (b) gauge, strain = 0.22; (c) gauge, strain = 0.44; (d) gauge, strain = 0.88.

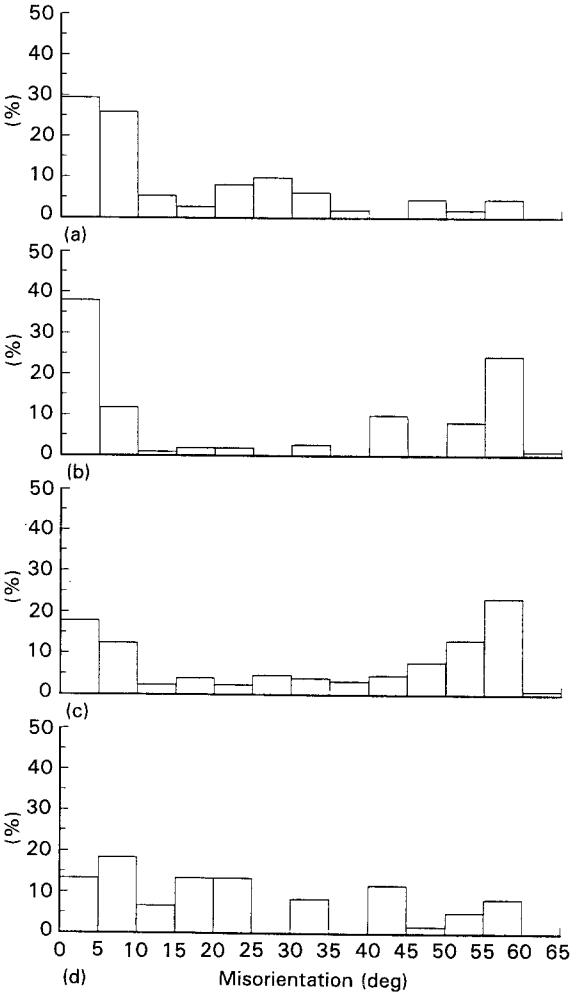

Figure 3 Experimentally determined boundary misorientation distributions for the grip and gauge sections of the Al–Cu–Li–Ag–Mg–Zr alloy. (a) Grip, strain = 0.21; (b) gauge, strain = 0.11; (c) gauge, strain = 0.21; (d) gauge, strain = 0.47.

of higher-angle boundaries, as a function of elevated temperature strain. At strains near 0.45, for example, boundaries with 10° or less misorientation represent fewer than one-third of the boundaries in each alloy. There are two potential origins for the observed shift in the boundary misorientation distributions. Either:

(i) some low-angle boundaries are transformed into high-angle boundaries as a result of (sub)grain rotation and (sub)grain switching processes; or

(ii) some of the low-angle boundaries initially present are eliminated by (sub)grain growth so that the high-angle boundaries initially present comprise a larger fraction of the total boundary population.

Examination of the boundary locations and orientations in transmission electron micrographs shows that explanation (i) is the dominant effect. For example, boundaries with misorientations between 10° and 20° and with the boundary plane approximately normal to the L direction are infrequently observed in the grip sections [21, 22]. After concurrent straining and annealing to $\varepsilon > 0.2$, such intermediate angle boundaries normal to the L direction are often observed. No evidence of discontinuous recrystallization was found in any of the grip or gauge sections.

While the boundary misorientation distributions provide a general picture of a shift from low misorientation angles to higher misorientation angles as a function of strain, the $\varepsilon = 0.88$ result for the Al–Cu–Zr–Si alloy illustrates the opposite trend. In a previous paper [22], evidence was presented to show that this effect was caused by a significant contribution to plastic deformation from intra(sub)granular slip in the strain interval 0.44–0.88. This results in reintensification of the original deformation texture and a shift of boundary misorientations back toward low angles. Modelling results pertinent to this case are presented later.

The combined experimental observations indicate that lattice rotations occur in all three of the alloys during the course of concurrent straining and annealing, but not during static annealing. This is consistent with the view of continuous recrystallization as a strictly dynamic process. However, the mechanism of lattice rotation is not clarified by these observations. In Section 3, simulative models of lattice rotation mechanisms are described and are applied to experimentally determined microstructure/microtexture states. In Section 4, model results are compared with experimental observations.

3. Boundary misorientation evolution models

Two mechanisms of (sub)grain rotation have been considered in the present study: (sub)grain rotation resulting from boundary sliding (BSSR), and from dislocation glide (DGSR). A simulative model of each process has been formulated, as described below. In addition, a (sub)grain neighbour switching analysis has been used to examine the effects of (sub)grain neighbour changes associated with boundary sliding.

To exercise the simulative models, an initial microstructure/microtexture state must be specified for each alloy. In the present investigation, measured (sub)grain positions, boundary positions, and lattice orientations from the grip sections of tensile specimens strained to $\varepsilon = 0.21$ or 0.22 are used to define the initial states. The boundary misorientation distributions for the microstructural states used for the three alloys are shown in Figs 1–3. Micrographs showing the boundary positions and misorientations have been previously published for the Al–Zr–Si and Al–Cu–Zr–Si alloys [21, 22]. The micrograph in Fig. 4a shows the (sub)grain structure found in the grip section of the Al–Cu–Li–Ag–Mg–Zr alloy. The misorientation angles of many of the boundaries in Fig. 4a are marked on the micrograph.

The grip sections of the tensile specimens have experienced the same thermal treatment as the gauge sections, but have not been strained. Total exposure time of each grip section at the test temperature is approximately 1000 s: the thermal stabilization period accounting for the first 600 s (approximately) and the remainder associated with the time required to attain a strain of 0.21 or 0.22 in the gauge section. During the straining process, the gauge sections of the tensile specimens are subject to both static annealing processes and dynamic processes associated with concurrent straining and annealing. However, the simulative models only account for dynamic processes. Using the grip-section microstructure/microtexture observations to define the initial states for the simulative models thus incorporates static annealing effects into the model results. For the alloys included in the present study, static annealing processes are slow compared to the dynamic processes of interest and little difference would be expected in the modelling results if microstructure/microtexture observations from the cold- or warm-rolled sheets were used to define the initial states for modelling purposes.

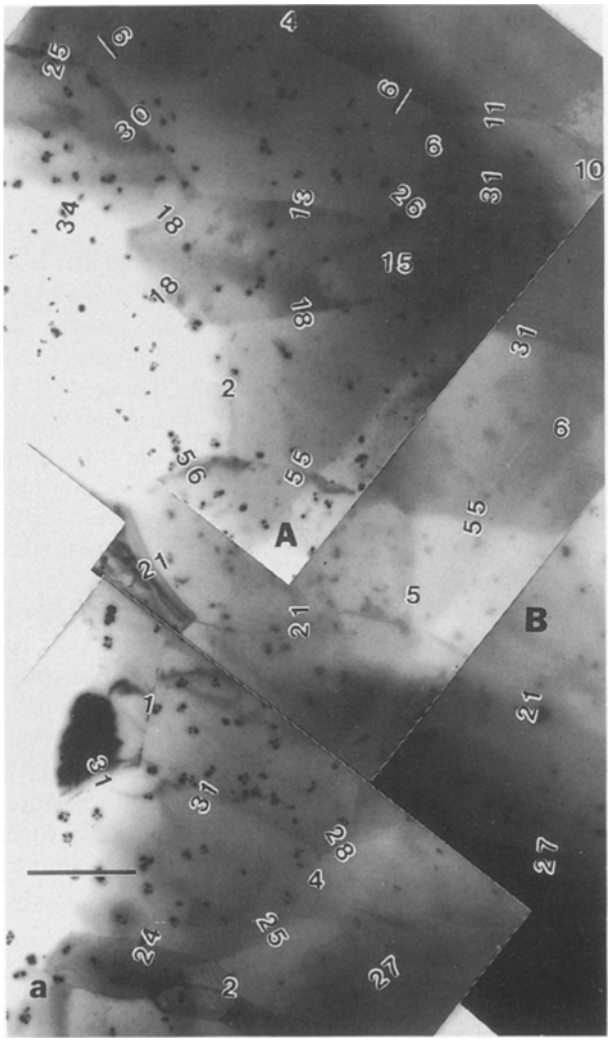

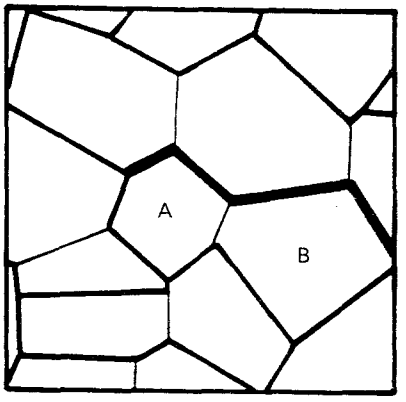

(b)

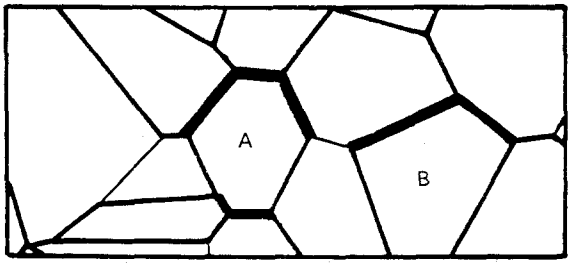

(c)

Figure 4 Method used to define (sub)grain neighbours after (sub)grain neighbour switching. (a) Transmission electron micrograph of the grip section of an Al–Cu–Li–Ag–Mg–Zr tensile specimen (gauge section strain = 0.22). Numbers marked on the micrograph represent boundary misorientation angles. The scale marker is parallel to L; T is normal to the page. (b) Dirichlet tessellation representing a portion of the microstructure in (a). Line thickness indicates boundary misorientation: thin lines represent 10° or less misorientation, intermediate lines represent boundary misorientations between 10° and 50°, and thick lines represent boundaries with misorientations of 50° or greater. (c) Dirichlet tessellation from (b) with centroid of each grain mapped to a new location corresponding to a tensile strain of 0.41.

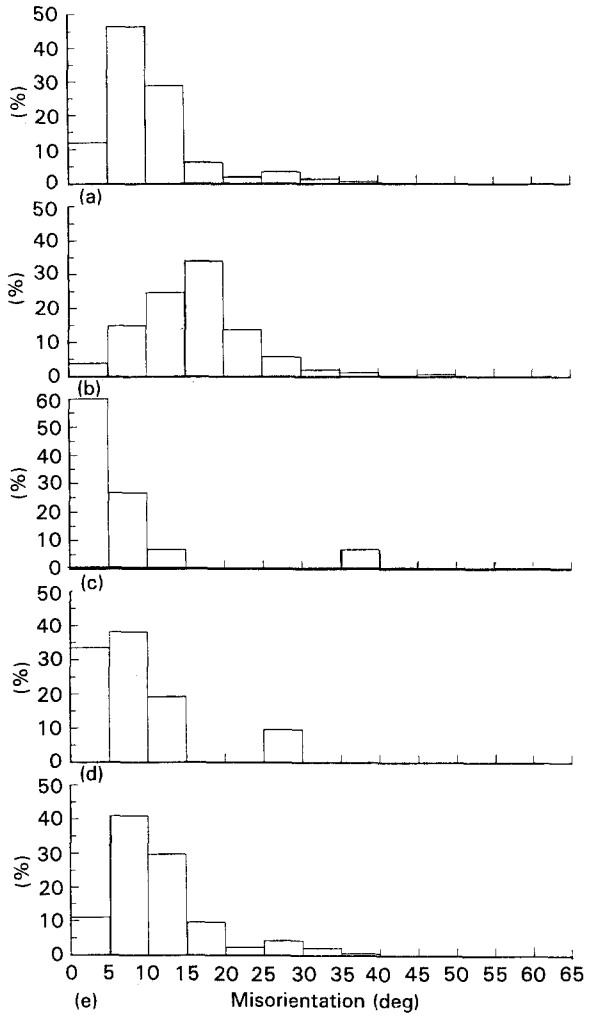

Figure 5 Calculated boundary misorientation distributions for the gauge sections of the Al–Zr–Si alloy. (a) 5° rotation; (b) 10° rotation; (c) intra (sub)granular slip; (d) switching; (e) 5° rotation + switching.

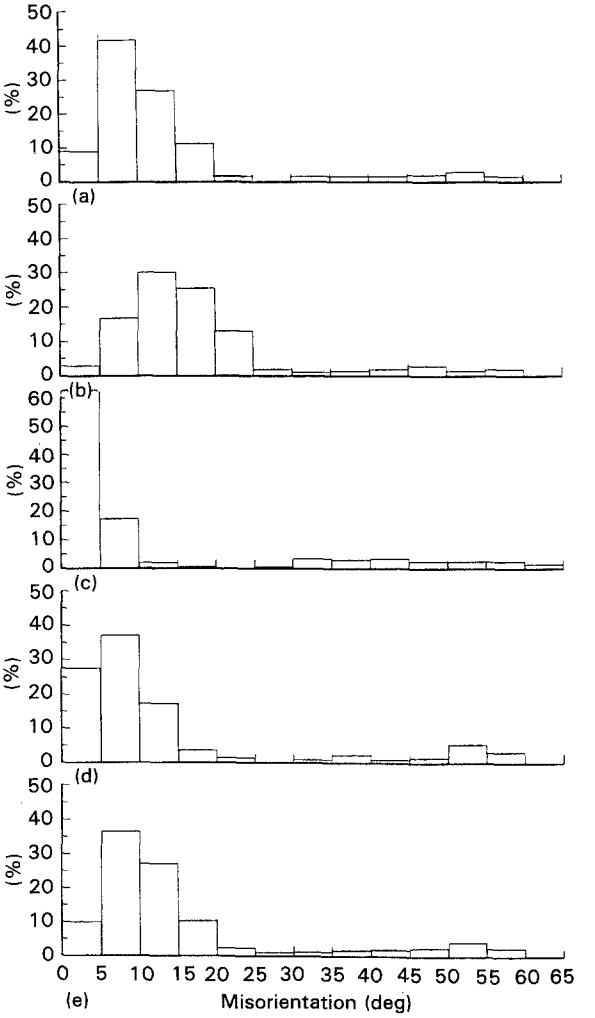

Figure 6 Calculated boundary misorientation distributions for the gauge sections of the Al–Cu–Zr–Si alloy. Model parameters for (a)–(e) are as in Fig. 5.

3.1. Boundary sliding (sub)grain rotation model

Grain rotation associated with boundary sliding has long been recognized as a characteristic feature of superplastic deformation [38–44]. Simulative modelling by Beere [43, 44] indicates that grain rotation accompanies boundary sliding even if all of the boundaries slide at the same rate. Differences in sliding rate among the various boundaries enveloping a grain, a result of differing boundary misorientations for example, strongly increases the rate of grain rotation in Beere's model.

The prior experimental observations and modelling results suggest that (sub)grain rotation occurs if boundary sliding contributes appreciably to the total strain. However, bicrystal boundary sliding experiments have consistently shown that low-angle boundaries slide at very low rates [45–50]. Therefore, if the initial microstructures of the alloys under investigation contained only low-angle boundaries, boundary sliding would be unable to contribute significantly to deformation and subgrain rotation associated with boundary sliding would not be expected. However, the boundary misorientation distributions presented in the previous section show that some of the boundaries present initially have high misorientation angles. It is proposed that sliding along these prior high-angle boundaries is sufficient to start the process of (sub)grain rotation in the adjacent (sub)grains [22]. Lattice rotation in (sub)grains initially bounded by at least one high-angle boundary introduces new high-angle boundaries, which start to slide as their misorientation exceed about 10°. In this view, continuous recrystallization is a cascade-like process that starts from high-angle boundaries initially present in the deformation microstructure.

Although the lattice rotation processes described above are inhomogeneous, these processes may be approximately simulated by imposing a lattice rotation on each (sub)grain. Examination of micro-pole figures from previous studies [21, 22] indicates that (sub)grain rotations up to 10° or 15° are induced by strains in the range 0.4–0.5. To simulate these lattice rotations, the BSSR model rotates the lattice of each (sub)grain by X degrees about a different, randomly selected axis. For purposes of the present study, $0° < X \leqslant 10°$.

To implement this procedure, the initial lattice orientation in each (sub)grain is specified by the experimentally determined orientation matrix that

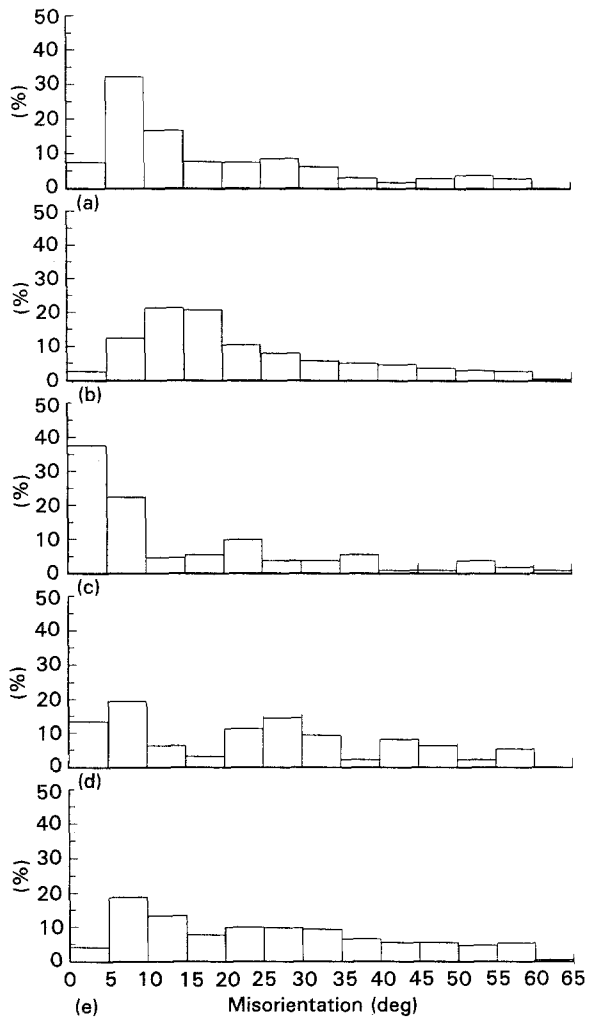

Figure 7 Calculated boundary misorientation distributions for the gauge sections of the Al–Cu–Li–Ag–Mg–Zr alloy. Model parameters for (a)–(e) are as in Fig. 5.

prescribes the lattice orientation relative to the bulk specimen axes: L, T and S. For each (sub)grain, a rigid body rotation matrix is constructed [51] using a randomly selected rotation axis and the specified angle of rotation, X. Matrix multiplication methods give new orientation matrices for the (sub)grains after rotation, from which new boundary misorientations are derived. Application of the simulative BSSR model to the initial lattice orientations for the three alloys included in the present investigation yields the boundary misorientation distributions shown in the upper two histograms in Figs 5–7.

3.2. Dislocation glide (sub)grain rotation model

Deformation texture is a result of slip on selected sets of slip systems within each grain. If intra(sub)granular slip contributed significantly to strain during concurrent straining and annealing of the tensile specimen gauge sections, the resulting lattice rotations would alter the boundary misorientation distributions. Lattice rotations resulting from dislocation glide are the basis for the DGSR model.

Taylor analyses require that five independent slip systems operate within each grain during plastic flow [52]. When five slip systems operate, calculations of the contribution of each slip system to strain and to lattice rotation are relatively complex. More recent analyses have shown that relaxed constraint models of texture development [53], in which fewer than five slip systems operate in each grain, are often in better agreement with experimental texture observations.

For the alloys used in the present investigation, bulk texture measurements show that the deformation texture resulting from cold- or warm-rolling is such that $< 1\,1\,2 >$ is approximately aligned with the rolling direction. Because the tensile axis and rolling direction coincide, the tensile axis is nearly parallel to $< 1\,1\,2 >$ for most (sub)grains. Schmid factor calculations show that the primary and conjugate slip systems for a $< 1\,1\,2 >$ tensile axis have Schmid factors substantially higher than the other ten slip systems. Therefore, we make the simplifying assumption that only the primary and conjugate slip systems operate in each (sub)grain, which permits use of an analytical treatment of duplex slip [54] to obtain the lattice rotation associated with dislocation glide as a function of tensile strain. Application of the DGSR model to the initial lattice orientations introduces a strain dependence in the orientation matrix components for each (sub)grain. Thus, the boundary misorientation distributions can be determined for selected strains. The boundary misorientation distributions obtained for a strain of 0.41 (tensile elongation = 50%) are represented in the middle histograms in Figs 5–7.

3.3. (Sub)grain neighbour switching model

The association between the boundary sliding process and grain neighbour switching is vividly conveyed by Fig. 4 in [55], which schematically illustrates the grain neighbour switching process for an idealized grain geometry. Even from such idealized illustrations it is clear that grain neighbour switching can alter the boundary misorientation distribution, independent of lattice rotations that may occur. However, determining which grains will be neighbours in a real microstructure after some amount of strain is not simple. To evaluate the magnitude of this effect, a simulative model for (sub)grain neighbour switching has been formulated.

In the model of (sub)grain neighbour switching, it is necessary to predict which (sub)grains in the initial microstructure will be neighbours after a selected strain. This prediction is made starting with a bright-field transmission electron micrograph from the grip section of a tensile specimen, Fig. 4a for example. The approximate x–y position of each (sub)grain centroid is determined for the (sub)grains in the micrograph. The group of (sub)grains selected for the analysis must form a contiguous region. The Dirichlet tessellation is computed using the (sub)grain centroids as the generating centres [56], Fig. 4b for example. To ensure that the Dirichlet tessellation provides an acceptable description of the microstructure, the list of (sub)grain neighbour pairs identified using the Dirichlet analysis is compared with the neighbour pair list identified

directly from the bright-field transmission electron micrograph. In the absence of markedly concave grains, (sub)grain neighbour pairs identified using the Dirichlet analysis match those identified directly from the micrograph.

To simulate the effect of strain on the microstructure, a homogeneous, area-preserving, plane strain corresponding to the desired tensile elongation is then imposed on the group of (sub)grain centroids, causing them to be mapped to new locations. The Dirichlet tessellation is recomputed using these new centroid locations, and new (sub)grain neighbours are identified for the selected strain level, Fig. 4c for example. The orientation matrix for each (sub)grain is unchanged as a result of this (sub)grain neighbour switching process, but the boundary misorientations are changed as a result of (sub)grain neighbour switching. Grains labelled A and B in Fig. 4 illustrate the effect that (sub)grain neighbour switching can have on the boundary misorientation distribution. Initially, these (sub)grains are neighbours separated by a 5° misorientation boundary. After straining, (sub)grains A and B are no longer neighbours and the low-angle boundary that initially separated them is absent from the boundary misorientation distribution. Note that the cells of the Dirichlet tessellation are approximately equiaxed following deformation, which is in accord with grain morphology observations for superplastically deformed materials [38–41]. The fourth histogram in Figs 5–7 shows the effect of (sub)grain neighbour switching on the boundary misorientation distributions for the three alloys included in the present study.

4. Discussion: comparison of experimental and model results

The effect of concurrent straining and annealing on boundary misorientation distributions has been established experimentally (Section 2) and through several simulative models (Section 3). The purpose of this discussion section is to compare the experimental and modelling results, with the goal of identifying which models most closely reproduce the experimental results. The models for DGSR and for (sub)grain neighbour switching are explicit functions of strain. The strain value used to obtain the modelling results shown in Figs 5–7 is 0.41. It is therefore appropriate to compare the modelling results with the experimental results for tensile specimens deformed to a similar strain. Figs 1–3 contain boundary misorientation distributions for tensile strains in the range 0.44 to 0.47 for the various alloys.

4.1. Boundary sliding (sub)grain rotation model results

For all three alloys, the prominent effect of the BSSR model on the boundary misorientation distribution is to decrease the fraction of boundaries with misorientations of 10° or less. Thus, the BSSR model reproduces the principal characteristic of the experimental boundary misorientation distributions for tensile strains near 0.45. For the Al–Zr–Si alloy, a rotation of 10° yields better agreement between the BSSR model results and the experimental boundary misorientation distribution, while a 5° rotation yields better agreement for the other two alloys.

Although the BSSR model reproduces in a general way the principal characteristic of the experimental observations, a strong fundamental basis for selecting a particular value of (sub)grain rotation to associate with strains near 0.45 does not exist. Previously published micro-pole figures for the Al–Zr–Si and Al–Cu–Zr–Si alloys [21, 22] show that initially similar (sub)grain orientations diverge during concurrent straining and annealing by rotations of up to 10° or 15°. The classic marker line experiments described by Matsuki *et al.* [40, 41] and others [42] reveal grain rotations of similar magnitude for strains near 0.5. In addition, the simulative grain rotation model formulated by Beere [43, 44] indicates that grain rotations of 10° or more are readily achieved at a strain of 0.5, provided that moderate differences in boundary sliding rate exist among the various boundaries in the material. Based on these observations, a rotation of 5° has been selected to represent the average subgrain rotation at a strain of 0.41.

The present (sub)grain rotation model uses the simplistic assumption that every (sub)grain rotates by the same amount, although the rotation axis is different for every (sub)grain. Even a 5° rotation from the initial (sub)grain orientations is sufficient to reduce the fraction of boundaries with misorientations of 10° or less. Such a reduction is characteristic of the experimental observations for all three alloys at strains below 0.5. A refined model in which the amount of (sub)grain rotation is randomly selected within some range might be able to improve detailed agreement between the experimental and model boundary misorientation distributions. However, it is important to remember that the experimental results are highly variable owing to the limited number of observations and to the inherent microstructural inhomogeneity. Thus, excessive refinement of the model(s) in an attempt to improve detailed agreement with the experimental observations does not appear to be warranted.

4.2. Dislocation glide (sub)grain rotation model results

Application of the DGSR model to the initial boundary misorientation distributions for the three alloys increases the fraction of boundaries with misorientations of 10° or less. This reflects convergence of (sub)grain orientations and intensification of the initial texture, a result that would be anticipated for deformation by slip. Because this result is contrary to experimental observations for strains near 0.45, we conclude that (sub)grain rotation during concurrent straining and annealing of the alloys studied in the present investigation is not a result of slip. This is consistent with an earlier report that the contribution of slip to the total strain was less than 10% during superplastic deformation of a continuously recrystallized Al–Cu–Zr alloy [26].

As noted in a previous paper [22], the strain interval 0.44–0.88 increases the fraction of boundaries with misorientations of 10° or less, and intensifies the bulk deformation texture of the Al–Cu–Zr–Si alloy. Brooks *et al.* [22] suggested that these observations reflect an increasing contribution of slip to the total strain in the interval 0.44–0.88. The DGSR model confirms that this is the expected result for deformation by slip, providing further support for the suggestion of Brooks *et al.* It is notable that the Al–Cu–Zr–Si alloy did not exhibit the large elongation characteristic of superplastic alloys. The limited elongation to failure is consistent with the view that intra(sub)granular slip processes were important in the strain interval 0.44–0.88, because alloys that deform predominately by slip are generally not superplastic. It is not known why this alloy deformed by mechanisms that produced divergent (sub)grain rotations during the strain interval 0–0.44, but shifted to mechanisms that produced convergent (sub)grain rotations during the strain interval 0.44–0.88.

4.3. (Sub)grain neighbour switching model results

(Sub)grain neighbour switching produced only modest changes in the boundary misorientation distributions for the three alloys. This result can be anticipated from knowledge of the initial microstructure/microtexture states of the alloys. (Sub)grains of similar orientation are arranged in deformation bands parallel to the rolling plane. Moderate elongation of deformation bands in the L direction maintains many (sub)grains of similar orientation in contact, with the result that (sub)grain neighbour switching does not strongly alter the boundary misorientation distributions.

4.4. Combined boundary sliding (sub)grain rotation and (sub)grain neighbour switching model results

The BSSR model produced boundary misorientation distributions broadly similar to those found experimentally. However, because the (sub)grains remain approximately equiaxed during deformation (a salient characteristic of superplastic deformation [38–41]), (sub)grain neighbour switching must occur in conjunction with the boundary sliding and (sub)grain rotation. To model the combination of these processes, we have applied the individual BSSR and (sub)grain neighbour switching models successively to the initial boundary misorientation distributions. Because the models are independent, the order of application is immaterial.

The last histogram in Figs 5–7 shows the combined BSSR and (sub)grain neighbour switching model results. Comparing these distributions with the experimentally determined distributions for strains near 0.45 reveals broad similarities. Thus, we find that a combination of the boundary sliding (sub)grain rotation and (sub)grain neighbour switching models produces boundary misorientation distributions consistent with experimental observations for the three alloys included in the present study. This finding is also consistent with a wide variety of previous observations concerning evolution of microstructure and texture during concurrent straining and annealing of superplastic aluminium alloys [13–26]. The modelling results support the idea that continuous recrystallization is strictly a dynamic process in which the applied stress drives (sub)grain rotation such that initial (sub)grain orientations diverge during concurrent straining and annealing.

5. Conclusions

This study of simulative modelling of microstructure/microtexture evolution during concurrent straining and annealing of three aluminium alloys has lead to the following conclusions.

1. The boundary misorientation distributions for the three alloys included in the present study are broadly similar after annealing alone and after concurrent straining and annealing. Annealing alone does not significantly alter the boundary misorientation distribution, while concurrent straining and annealing decreases the fraction of low-angle boundaries.

2. Three simulative models of microstructure/microtexture evolution during concurrent straining and annealing have been formulated. Application of the models to experimentally determined initial microstructure/microtexture states shows that the boundary sliding (sub)grain rotation model decreases the fraction of low-angle boundaries, the dislocation glide (sub)grain rotation model increases the fraction of low-angle boundaries, and the (sub)grain neighbour switching model modestly decreases the fraction of low-angle boundaries.

3. A combination of the boundary sliding (sub)grain rotation model and the (sub)grain neighbour switching model most closely reproduces the boundary misorientation distributions found experimentally.

4. The experimental and modelling results are consistent with the view that continuous recrystallization is strictly a dynamic process.

Acknowledgements

The authors thank Dr S. Hales, Dr P. Kalu and Dr W. James, NASA Langley Research Center, for helpful discussions. B. Pham provided experimental assistance. Support for this work was provided by the NASA Langley Research Center under contract NAG 1-745.

References

1. H. HU, in "Recovery and Recrystallization of Metals", edited by L. Himmel (Gordon and Breach, New York, 1963) p. 311.
2. J. C. M. LI, *J. Appl. Phys.* **33** (1962) 2958.
3. R. D. DOHERTY and J. W. CAHN, *J. Less-Common Metals* **28** (1979) 279.
4. R. D. DOHERTY, in "Recrystallization of Metallic Materials", edited by F. Haessner (Riederer, Stuttgart, 1978) p. 23.

5. J. GREWEN and J. HUBER, *ibid.* p. 111.
6. B. M. WATTS, M. J. STOWELL, B. L. BAKIE and D. G. E. OWEN, *Met. Sci.* **10** (1976) 189.
7. *Idem, ibid.* **10** (1976) 198.
8. R. H. BRICKNELL and J. W. EDINGTON, *Met. Trans.* **10A** (1979) 1257.
9. *Idem, ibid.* **27** (1979) 1303.
10. E. NES, *J. Mater. Sci. Lett.* **13** (1978) 2052.
11. *Idem, Met. Sci.* **13** (1979) 211.
12. *Idem*, in "Superplasticite/Superplasticity", edited by B. Baudelet and M. Suery (Editions du CNRS, Paris, 1985) p. 7.1.
13. T. R. McNELLEY, E.-W. LEE and M. E. MILLS, *Metall. Trans.* **17A** (1986) 1035.
14. E.-W. LEE, T. R. McNELLEY, A. F. STENGEL, *ibid.* **17A** (1986) 1043.
15. T. R. McNELLEY, E.-W. LEE and A. GARG, in "Aluminum Alloys-Physical and Mechanical Properties", edited by E. A. Starke and T. H. Sanders (Engineering Materials Advisory Services, West Midlands, 1986) p. 1269.
16. E.-W. LEE and T. R. McNELLEY, *Mater. Sci. Eng.* **93** (1987) 45.
17. *Idem, ibid.* **96** (1987) 253.
18. S. J. HALES and T. R. McNELLEY, *Acta Metall.* **36** (1988) 1229.
19. *Idem*, in "Superplasticity in Aerospace", edited by H. C. Heikkenen and T. R. McNelley (TMS, Warrendale, PA, 1988) p. 61.
20. R. CROOKS, *ibid.*, p. 51.
21. H. GUDMUNDSSON, D. D. BROOKS and J. A. WERT, *Acta Metall. Mater.* **39** (1991) 19.
22. D. D. BROOKS, H. GUDMUNDSSON and J. A. WERT, in "Hot Deformation of Aluminum Alloys", edited by T. G. Langdon, H. D. Merchant, J. G. Morris and M. A. Zaidi (TMS, Warrendale, PA, 1991) p. 55.
23. A. J. SHAKESHEFF, D. S. McDARMAID and P. J. GREGSON, *Mater. Sci. Technol.* **7** (1991) 276.
24. S. J. HALES, T. R. McNELLEY and H. J. McQUEEN, *Metall. Trans.* **22A** (1991) 1037.
25. A. W. BOWEN and J. HIRSCH, in "Eighth International Conference on Textures of Materials", edited by J. S. Kallend and G. Gottstein (TMS, Warrendale, PA, 1988) p. 549.
26. J. HIRSCH, K. A. PADMANABHAN, K. LUCKE, *ibid.*, p. 555.
27. N. A. GJOSTEIN and F. N. RHINES, *Acta Metall.* **7** (1959) 319.
28. G. HASSEN, M. BISCONDI, P. LAGARDE, J. LEVY and C. GOUX, *Surf. Sci.* **31** (1972) 115.
29. H. J. McQUEEN and J. E. HOCKETT, *Metall. Trans.* **1** (1970) 2997.
30. A. R. JONES, B. RALPH and N. HANSEN, *Proc. R. Soc. Lond. A* **368** (1979) 345.
31. A. R. JONES, in "Grain Boundary Structure and Kinetics" (ASM, Metals Park, OH, 1980) p. 379.
32. B. BAY and N. HANSEN, in "Recrystallization and Grain Growth Multiphase and Particle-Containing Materials", edited by N. Hansen, A. R. Jones and T. Leffers (Risø-National Laboratory, Risø, 1980) p.51.
33. N. HANSEN and B. BAY, *Acta Metall.* **29** (1981) 65.
34. A. R. JONES and N. HANSEN, *ibid.* **29** (1981) 589.
35. C. Y. J. BARLOW, B. BAY and N. HANSEN, *Philos. Mag. A* **51** (1985) 253.
36. E. NES, W. B. HUTCHINSON and A. A. RIDHA, in "Seventh International Conf. Strength of Metals and Alloys", edited by H. J. McQueen, J.-P. Bailon, J. I. Dickson, J. J. Jonas and M. G. Akben (Pergamon Press, Oxford, 1986) p. 57.
37. B. BAY, N. HANSEN and D. KUHLMANN-WILSDORF, *Mater. Sci. Eng.* **A113** (1989) 385.
38. J. W. EDINGTON, *Metall. Trans.* **13A** (1982) 703.
39. W. D. NIX, in "Superplastic Forming", edited by S. P. Agrawal (ASM, Metals Park, OH, 1985) p. 3.
40. K. MATSUKI, H. MORITA, M. YAMAUA and Y. MURAKAMI, *Met. Sci.* **11** (1977) 156.
41. K. MATSUKI, H. MINAMI, M. TOKIZAWA and Y. MURAKAMI, *ibid.* **13** (1979) 619.
42. A. E. GECKINLI and C. R. BARRETT, *J. Mater. Sci.* **11** (1976) 510.
43. W. BEERE, *ibid.* **12** (1977) 2093.
44. *Idem, Phil. Trans. R. Soc. Lond. A* **288** (1978) 177.
45. S. K. TUNG and R. MADDIN, *Trans. AIME* **209** (1957) 905.
46. F. WEINBERG, *ibid.* **212** (1958) 808.
47. M. BISCONDI and C. GOUX, *Mem. Sci. Rev. Metall.* **65** (1968) 167.
48. P. LAGARDE and M. BISCONDI, *Canad. Metall. Q.* **13** (1974) 245.
49. T. WATANABE, N. KURIYAMA and S. KARASHIMA, in "Proceedings of the Fourth International Conference on Strength of Metals and Alloys", Nancy, France, (1976) Vol. 1, p. 383.
50. Z. Q. ZHOU, B. L. WU and C. Q. CHEN, in "Aluminum Alloys'90, Proceedings of the Second International Conference on Aluminum Alloys – Their Physical and Mechanical Properties", edited by C. Q. Chen and E. A. Starke (International Academic, Bejing, 1990) p. 571.
51. H. K. D. H. BHADESHIA, in "Worked Examples in the Geometry of Crystals" (Chameleon Press, London, 1987) p. 18.
52. J. F. W. BISHOP and R. HILL, *Philos. Mag.* **42** (1951) 1298.
53. U. F. KOCKS and H. CHANDRA, *Acta Metall.* **30** (1982) 695.
54. C. N. REID, in "Deformation Geometry for Materials Scientists" (Pergamon Press, Oxford, 1973) p. 137.
55. M. F. ASHBY and R. A. VERALL, *Acta Metall.* **21** (1973) 149.
56. A. GETIS and B. BOOTS, in "Models of Spatial Processes" (Cambridge University Press, Cambridge, 1978) p. 126.

Received 9 February
and accepted 7 December 1993